AAC Journals.ASM.org

Induction of Mitochondrial Dysfunction and Oxidative Stress in *Leishmania donovani* by Orally Active Clerodane Diterpene

Manoj Kathuria,[a] Arindam Bhattacharjee,[a] Koneni V. Sashidhara,[b,c] Suriya Pratap Singh,[b] Kalyan Mitra[a,c]

Electron Microscopy Unit, Sophisticated Analytical Equipment Facility,[a] and Medicinal & Process Chemistry Division,[b] CSIR-Central Drug Research Institute, Lucknow, India; Academy of Scientific and Innovative Research, New Delhi, India[c]

This study was performed to investigate the mechanistic aspects of cell death induced by a clerodane diterpene (K-09) in *Leishmania donovani* promastigotes that was previously demonstrated to be safe and orally active against visceral leishmaniasis (VL). K-09 caused depolarization of the mitochondrion and the generation of reactive oxygen species, triggering an apoptotic response in *L. donovani* promastigotes. Mitochondrial dysfunction subsequently resulted in the release of cytochrome *c* into the cytosol, impairing ATP production. Oxidative stress caused the depletion of reduced glutathione, while pretreatment with antioxidant *N*-acetyl cysteine (NAC) was able to abrogate oxidative stress. However, NAC failed to restore the mitochondrial membrane potential or intracellular calcium homeostasis after K-09 treatment, suggesting that the generation of oxidative stress is a downstream event relative to the other events. Caspase-3/-7-like protease activity and genomic DNA fragmentation were observed. Electron microscopy studies revealed gross morphological alterations typical of apoptosis, including severe mitochondrial damage, pyknosis of the nucleus, structural disruption of the mitochondrion-kinetoplast complex, flagellar pocket alterations, and the displacement of organelles. Moreover, an increased number of lipid droplets was detected after K-09 treatment, which is suggestive of altered lipid metabolism. Our results indicate that K-09 induces mitochondrial dysfunction and oxidative stress-mediated apoptotic cell death in *L. donovani* promastigotes, sharing many features with metazoan apoptosis. These mechanistic insights provide a basis for further investigation toward the development of K-09 as a potential drug candidate for VL.

Leishmaniasis is a neglected tropical vector-borne disease caused by obligate intracellular protozoan parasites of the genus *Leishmania*. Infection with different species of this genus transmitted through sandfly vectors results in different manifestations of the disease, out of which visceral leishmaniasis (VL) or kala-azar caused by *Leishmania donovani*, is the most severe form and is often fatal. *Leishmania* spp. have digenetic life cycles involving a flagellated promastigote stage residing in the gut of the sandfly (*Phlebotomus* sp.) and a nonmotile intracellular amastigote stage found in mononuclear phagocytes in the bloodstream of an infected individual (1). Leishmaniasis affects populations from tropical to Mediterranean regions, inflicting a heavy burden of morbidity and mortality; according to World Health Organization estimates, 2 million new cases of leishmaniasis occur annually, with 500,000 cases of VL alone (see http://www.who.int/leishmaniasis/burden/magnitude/burden_magnitude/en/).

In the absence of any protective vaccination, chemotherapy remains the mainstay for treating leishmaniasis, along with effective management against secondary infections. The drugs used in the treatment regimen of VL include pentavalent antimonials, liposomal amphotericin B, paromomycin, and more recently, the only orally administered drug, miltefosine (2). These treatments face severe limitations due to their nonspecificity, toxicity, route of administration, cost-effectiveness, and the tendency to develop resistance (3). Therefore, there is an urgent need to develop new, cheap, and easy-to-administer drugs with better safety profiles. The drug discovery effort has now shifted heavily toward natural products, due to their limitless variety of novel skeletons for combinatorial modification and their low toxicity. It is interesting to note that ~75% of the drugs developed against infectious diseases have their origins in nature (4).

Apoptosis, a key mechanism for inducing programmed cell death (PCD), has been demonstrated in kinetoplastid protozoans and is no longer considered to be limited to multicellular organisms. Apoptosis is a controlled self-destructing and energy-dependent process exhibiting specific morphological and biochemical features, such as cell shrinkage, plasma membrane blebbing, loss of mitochondrial membrane potential, chromatin condensation, and nuclear fragmentation (46). Increasing experimental evidence shows that apoptosis-like programmed cell death pathways are functional in trypanosomatids (5). Apoptosis may be induced by various physiological (such as nutrient deprivation and heat shock) and chemical (H_2O_2 and chemotherapeutic agents, like camptothecin and miltefosine) stimuli (6–10). Although *Leishmania* organisms share many biochemical markers with metazoan apoptosis, the molecular machinery involved differs considerably and is not well understood. A better understanding of the mechanistic machinery of apoptosis-like PCD in protozoan protists thus would prove immensely beneficial in the design of rational chemotherapeutic interventions in a target-dependent manner.

In our ongoing efforts to identify and understand the modes of action of new and effective leishmanicidal agents, several natural products are currently being evaluated in our laboratory. Here, we report on the mechanistic aspects of a clerodane diterpene-induced cell death in *L. donovani*. In the present study, we investigated the physiological and ultrastructural alterations in *L. don-*

Received 5 February 2014 **Returned for modification** 6 May 2014
Accepted 18 July 2014
Published ahead of print 28 July 2014
Address correspondence to Kalyan Mitra, k_mitra@cdri.res.in.
M.K. and A.B. contributed equally to this work.
Copyright © 2014, American Society for Microbiology. All Rights Reserved.
doi:10.1128/AAC.02459-14

ovani promastigotes following the administration of a clerodane diterpenoid designated K-09 (16α-hydroxycleroda-3,13(14)*Z*-dien-15,16-olide) isolated previously from the leaves of *Polyalthia longifolia*. K-09 was previously reported to be an orally active antileishmanial agent working as a DNA topoisomerase inhibitor (11). Our studies reveal that it is capable of inducing promastigote cell death by mitochondrial dysfunction, reactive oxygen species (ROS) generation, elevation of cytosolic Ca^{2+}, and DNA fragmentation. Other apoptotic features, such as externalization of phosphatidylserine and caspase-like protease activity, were also observed, along with an increase in the number of cytoplasmic lipid droplets.

MATERIALS AND METHODS

Drugs and chemicals. A silica gel column chromatography-purified compound (16α-hydroxycleroda-3,13(14)*Z*-dien-15,16-olide), designated K-09, from the hexane extracts of *P. longifolia* leaves, was obtained as reported earlier (11). A stock solution of 5 mg/ml (15.7 mM) was prepared in dimethyl sulfoxide (DMSO) and stored at −20°C. *N*-acetyl cysteine, miltefosine, ionomycin, oligomycin A, and Triton X-100 were purchased from Calbiochem, Darmstadt, Germany. JC-1, 5(6)-carboxy-2′,7′-dichlorodihydrofluorescein diacetate (carboxy-H_2DCFDA), fluo-4 acetoxymethyl ester (Fluo-4 AM), probenecid, MitoTracker deep red, MitoSOX red, and Nile red were from Molecular Probes (Eugene, OR, USA). All other chemicals were from Sigma-Aldrich (MO, USA), unless otherwise stated.

Cell culture and treatments. *L. donovani* (strain MHOM/IN/80/DD8) promastigotes were cultured, as described previously, in Dulbecco's modified Eagle's medium (DMEM) supplemented with 10% fetal bovine serum (FBS) and gentamicin (40 μg/ml) at 26°C (12). After the cell density had reached ~10^6 cells/ml, the parasites were prepared for drug treatment in fresh medium. K-09 was administered at concentrations of 8 μg/ml (50% inhibitory concentration [IC_{50}], 25 μM) and 16 μg/ml (2× the IC_{50}, 50 μM) and incubated for 24 h at 26°C. Vehicle control (VC) cells were incubated at the same DMSO concentration as with the K-09 treatments (0.001% [vol/vol]). J774A.1 murine macrophages were cultured and infected with *L. donovani* promastigotes, as described earlier (11).

Ultrastructural analysis by transmission electron microscopy. The cells were fixed with 4% paraformaldehyde (PFA) and 2% glutaraldehyde in 0.1 M phosphate buffer (pH 7.4) for 4 h at room temperature (RT). The samples were then washed in 0.1 M phosphate buffer, postfixed in 2% OsO_4, and encapsulated in agarose. This was followed by dehydration in ascending grades of ethanol, infiltration, embedding in an Epon 812-araldite plastic mixture, and polymerization at 60°C for 24 h. Ultrathin sections (50 to 70 nm) were obtained using an ultramicrotome (Leica Ultracut UCT; Leica Microsystems GmbH, Wetzlar, Germany) and picked up onto 200 mesh copper grids. The sections were double stained with uranyl acetate and lead citrate and observed under a FEI Tecnai-12 twin transmission electron microscope equipped with a SIS MegaView II CCD camera at 80 kV (FEI Company, Hillsboro, OR, USA). At least 400 cells were analyzed in the experiments.

Analysis of topological alterations by scanning electron microscopy. The cells were fixed in 2.5% glutaraldehyde in 0.1 M phosphate buffer. After washing in phosphate buffer, the suspensions were placed on poly-L-lysine-coated glass chips and allowed to adhere for 10 min at room temperature (RT). The samples were postfixed in 1% OsO_4 and subsequently dehydrated through an ascending ethanol series, were critical point dried, and were coated with Au-Pd (80:20) using a Polaron E5000 sputter coater. The samples were examined in an FEI Quanta 250 scanning electron microscope (SEM) at an accelerating voltage of 10 kV, using the SE detector. Micrographs were taken at magnifications of ×5,000 and ×10,000. About 200 cells from two stubs for each sample were analyzed. The flagellar length and parasite body length of at least 100 cells were measured with the xT Microscope Control software (FEI).

Confocal microscopy and image analysis. The slides were analyzed under a Carl Zeiss LSM 510 Meta confocal laser scanning microscope (Carl Zeiss, Jena, Germany) equipped with a 405-nm diode, argon multiline (458, 477, 488, and 514 nm), 561-nm diode-pumped solid state (DPSS), and HeNe 633-nm lasers. A Plan-Apochromat 63×/1.4-numerical-aperture (NA) oil differential interference contrast (DIC) objective lens was used with appropriate excitation and emission filters for imaging. Quantitative analysis of the images was performed using Zeiss AIM version 4.2.

Fluorometric studies. Prior to taking fluorometric measurements, the cells (10^7/ml) were transferred in 96-well flat-bottom fluorescence measurement microplates. All experimental data, unless stated otherwise, were collected with a Tecan Infinite M1000 PRO monochromator-based fluorescence microplate reader (Tecan Group, Ltd., Männedorf, Switzerland) with top reading, a bandwidth of 5.0 nm, and gain set to optimal.

Measurement of changes in mitochondrial membrane potential. K-09-induced changes in the mitochondrial membrane potential ($\Delta\Psi_m$) were measured by the mitochondrial membrane-permeable cationic potentiometric vital dye JC-1, which deposits in a ratiometric manner as J-aggregates in the mitochondria of cells with higher $\Delta\Psi_m$, giving red (590 nm) fluorescence (indicating healthy cell), and it remains as a green monomer in the cytoplasm of cells with depolarized mitochondria (i.e., depleted $\Delta\Psi_m$, indicating apoptotic cells). Briefly, after harvesting, 2 μM JC-1 was added to the VC and treated cells that were then incubated in darkness for 20 min on poly-L-lysine-coated coverslips, mounted, and imaged immediately by confocal microscopy. In a subset of VC cells, oligomycin-A (oli-A) (an inhibitor of the F_oF_1 ATPase complex) or 50 μM carbonyl cyanide *m*-chlorophenylhydrazone (CCCP) (a respiratory uncoupler) was added 1 h prior to the addition of JC-1. The excitation line was 488 nm, and the emission filters were a band pass (BP) of 505 to 550 nm (green) and a long pass (LP) of 575 nm (red). The mean fluorescence intensity in each emission channel was measured for ≥20 cells for each case, and the 530/590 nm ratio was calculated.

Following drug treatment, a subset of the cells was subjected to flow cytometry in a BD FACSCalibur flow cytometer (Becton Dickinson, Franklin Lakes, NJ, USA), with 488 nm excitation and emission filters of 525 ± 15 nm and 570 ± 25 nm for the green and red channels, respectively. The data were analyzed with the CellQuest Pro software, taking 10,000 events as the standard.

Depolarization of the mitochondrion was tracked in real time by taking kinetic fluorescence measurements. The cells, which were prestained with 2 μM JC-1, were treated or not with K-09 and CCCP against the VC and immediately tracked in the fluorometer (530 nm) for 1.5 h. To test the effect of ROS quenching, pretreatment with 20 mM *N*-acetyl cysteine (NAC) (for 2 h) was given before K-09 treatment, and kinetic measurements were performed.

Estimation of mitochondrial superoxide levels. Mitochondrial superoxide levels were estimated with MitoSOX red, a fluorogenic dye specific for mitochondrial superoxide, which is cleaved after reacting with O_2^- produced by the mitochondria, and it emits red fluorescence upon binding with DNA. The experiment was performed according to the manufacturer's instructions. Confocal microscopy of the cells treated with the IC_{50} of K-09, 2× the IC_{50} of K-09, and the VC cells was performed by adding 5 μM MitoSOX red solution in phosphate-buffered saline (PBS) to the cells that adhered to poly-L-lysine-coated coverslips and allowed to incubate for 15 min at RT, followed by confocal imaging. Flow cytometry analysis of the above set of cells (10^7/ml) was also performed according to the above protocol, keeping the cells in suspension prior to analysis.

Monitoring of changes in intracellular Ca^{2+} levels. Changes in the intracellular calcium levels were measured by the fluorometric dye fluo-4 acetoxymethyl ester (Fluo-4 AM). Fluo-4 AM is a cell-permeant ester that shows large fluorescence yields upon binding intracellular Ca^{2+}. The experiment was performed as described previously (13), with the following

modifications. The cells were treated with the IC_{50} of K-09 and pretreated with 2 mM EGTA (2 h) before K-09 treatment and with the calcium ionophore ionomycin (5 μM). Next, the cells were incubated (45 min at RT) in a cocktail of 5 μM Fluo-4 AM, 1 μM Pluronic F-127, for permeabilization of the dye, and 2 mM probenecid, which prevents Ca^{2+} leakage from cells. After incubation, the cells were washed twice in PBS to remove nonhydrolyzed dye and were adhered to poly-L-lysine-coated coverslips before visualization with confocal microscopy. To observe the changes in cytosolic Ca^{2+} levels in real time, the cells were prestained with Fluo-4 AM as described earlier and then treated with the IC_{50} of K-09, 2× the IC_{50} of K-09 in the presence of EGTA in the medium (2 mM), and with ionomycin immediately prior to taking kinetic fluorescence measurements. In another set, NAC pretreatment was given before K-09 treatment and was processed as mentioned earlier.

Measurement of ROS levels. The fluorogenic marker 5(6)-carboxy-2′,7′-dichlorodihydrofluorescein diacetate (carboxy-H_2DCFDA) was used for this study, which is a live-cell-permeable acetate ester, and upon entry, it is cleaved by cellular esterases and reacts with cellular ROS (generated heavily during periods of oxidative stress) to emit fluorescence in the green region by converting into actively fluorescing dichlorofluorescein (DCF). Cellular ROS is quenched by NAC, an amino acid with potent antioxidant capabilities. The cells were treated with the IC_{50} of K-09 with or without 20 mM NAC pretreatment (for 2 h) and with 5 mM *tert*-butyl hydroperoxide (TBHP), a known ROS-inducing agent. The cells were then washed once in PBS and adhered to poly-L-lysine-coated coverslips, followed by incubation with 10 μM carboxy-H_2DCFDA (for 30 min) solution in darkness at RT before processing for confocal imaging.

Kinetic fluorometric studies were similarly performed to assess the rate of ROS generation following treatment, as well as the effect of NAC on ROS quenching. The cells were prestained with carboxy-H_2DCFDA and then treated with the IC_{50} of K-09 with or without NAC pretreatment as well as TBHP immediately before taking fluorescence measurements.

Measurement of reduced glutathione levels. During PCD, the elevated generation of free radicals is buffered by the intracellular thiol buffer system, the main component of which is the tripeptide glutathione. It exists in reduced (GSH) and oxidized (GSSG) forms, with the levels of GSH being drastically reduced in the presence of oxidative stress. Reduced glutathione is stained by bimane dyes, such as monochlorobimane (14). The cellular glutathione levels were measured with the ApoAlert glutathione assay kit (Clontech, Mountain View, CA, USA) according to the manufacturer's instructions, with minor modifications. Briefly, the cells were harvested, lysed with the provided lysis buffer, and centrifuged, and the supernatant was collected; this was then incubated with 2 mM monochlorobimane (MCB) at 37°C for 3 h in the dark. Sample fluorescence was subsequently analyzed on a FLUOstar Omega microplate reader (BMG Labtech, Ortenberg, Germany).

Determination of mitochondrial morphology by MitoTracker deep red staining. Physical disruption of the parasite mitochondria was investigated with MitoTracker deep red. MitoTracker dyes are a class of cell-permeable fluorescent probes that are based on a mildly thiol-reactive chloromethyl moiety specific for staining mitochondria. Briefly, after treatment with the IC_{50} of K-09 and CCCP treatment, the cells were harvested, washed once with PBS, immobilized to poly-L-lysine-coated coverslips, and incubated with 100 nM MitoTracker deep red (for 20 min at RT) before imaging.

Detection of cytochrome *c* release from mitochondria by immunofluorescence microscopy. Cytochrome *c* release occurs after the opening of the mitochondrial permeability transition pore (MPTP) and activates the downstream effectors, such as the initiator caspases. The microscopic localization of cytochrome *c* was performed as described previously (9). Briefly, cells with or without drug treatments were fixed in 4% PFA, permeabilized with 0.1% Triton X-100, and adhered to coverslips. Afterwards, the cells were incubated with anti-cytochrome *c* primary antibody (catalog no. sc-7159; Santa Cruz Biotechnology, Dallas, TX, USA) overnight at 4°C and subsequently with fluorescein isothiocyanate (FITC)-labeled secondary antibody (catalog no. GX-5011FC3R; Genetix Biotech, New Delhi, India) for 2 h at RT and processed for confocal imaging.

Measurement of intracellular ATP levels. The depletion of the intracellular ATP pool following drug treatment was monitored by employing the firefly luciferase bioluminescence-based ATP detection assay (ATP determination kit; Invitrogen) (15). Briefly, the VC and K-09-treated cells (10^7/ml) were harvested by pelleting, resuspended with boiling distilled water, and were further boiled for 5 min for lysis. The supernatant was added to the reaction mixture (1:19) (1 mM dithiothreitol [DTT], 0.5 mM D-luciferin, 20× assay buffer, 1.25 μg/ml firefly luciferase), incubated for 10 min at 28°C, and read in a Bio-Tek FLx 800T microplate reader (Bio-Tek, Winooski, VT, USA).

Oli-A (10 μM) treatment (until harvesting of cells) in promastigotes and amastigotes was given 2 h after K-09 treatment in the presence of low- (1 mg/ml) and high-glucose (4.5 mg/ml) media. Whether the addition of oli-A after K-09 exposure increased cell viability in *Leishmania* promastigotes in the presence or absence of glycolytic substrate glucose was measured using the CCK-8 cell counting kit (Dojindo Laboratories, Kumamoto, Japan).

Imaging and quantification of cytoplasmic lipid droplets. Altered lipid metabolism during periods of stress might affect the quantity of lipid storage bodies (lipid droplets [LDs]) inside the cell, which is revealed by quantifying and comparing intracellular LDs pre- and posttreatment. The fluorescent lysochrome dye Nile red (NR), which selectively stains intracellular lipid droplets, was used for this study (16). Briefly, the VC and K-09-treated cells were harvested, washed once with PBS, and stained with NR (1 μg/ml) for 10 min at RT, followed by immobilization on poly-L-lysine-coated coverslips and visualization under a confocal microscope. The mean number of LDs was calculated from ≥20 cells.

Detection of caspase-3/-7 activity. A major feature of apoptotic death is the involvement of cysteine aspartate proteases (caspases) that mediate events downstream of the mitochondria (17). The activities of caspases-3 and -7, two major executioner caspases, were monitored following treatment with the NucView 488 caspase-3 assay kit (Biotium, Hayward, CA, USA), according to the manufacturer's protocol. The assay uses an inactivated DNA dye excited by a 488 nm laser, which is tagged with the tetrapeptide caspase-3 recognition sequence DEVD (Asp-Glu-Val-Asp). Upon cleavage by caspase-3 (or its homologues), the NucView substrate binds to cellular DNA and yields the active green fluorescent product; the unbound dye is nonfluorescent and is washed away. Cells treated or not with the IC_{50} of K-09 and with or without the caspase-3/-7 inhibitor Ac-DEVD-CHO (10 μM; 2 h pretreatment) were used in the experiment. Briefly after harvesting, the cells were incubated with 5 μM NucView 488 substrate (for 30 min at RT) and thereafter immobilized on poly-L-lysine-coated coverslips for imaging.

Detection of phosphatidylserine reversal by microscopy. The reversal of phosphatidylserine (PS) from the inner to the outer leaflet of the plasma membrane is a characteristic early feature of apoptosis in *Leishmania* (10). To test this, we used FITC-tagged annexin V, a protein that binds to externalized phosphatidylserine. The experiment was performed according to the manufacturer's protocol (ApoDetect annexin V-FITC kit; Invitrogen). The cells treated or not with the IC_{50} of K-09 and cells preincubated with 10 μM caspase inhibitor Ac-DEVD-CHO (2 h pretreatment) were harvested, washed, and resuspended in 1× binding buffer. The annexin V-FITC antibody mixture was added and incubated for 10 min at RT. The cells were then washed once with binding buffer, adhered to poly-L-lysine-coated coverslips, and processed for confocal imaging.

Cell cycle analysis by flow cytometry. DNA content analysis was performed using propidium iodide (PI). Briefly, the cells with and without treatment were harvested and fixed in 70% ethanol (for 1 h at 4°C). Afterwards, the cells were pelleted, washed with PBS, and then resuspended in 300 μl of PBS. Next, 35 μl of RNase A (10 mg/ml stock) was added to the cells and kept at 37°C for 30 min. Subsequently, 10 μl of PI (1 mg/ml)

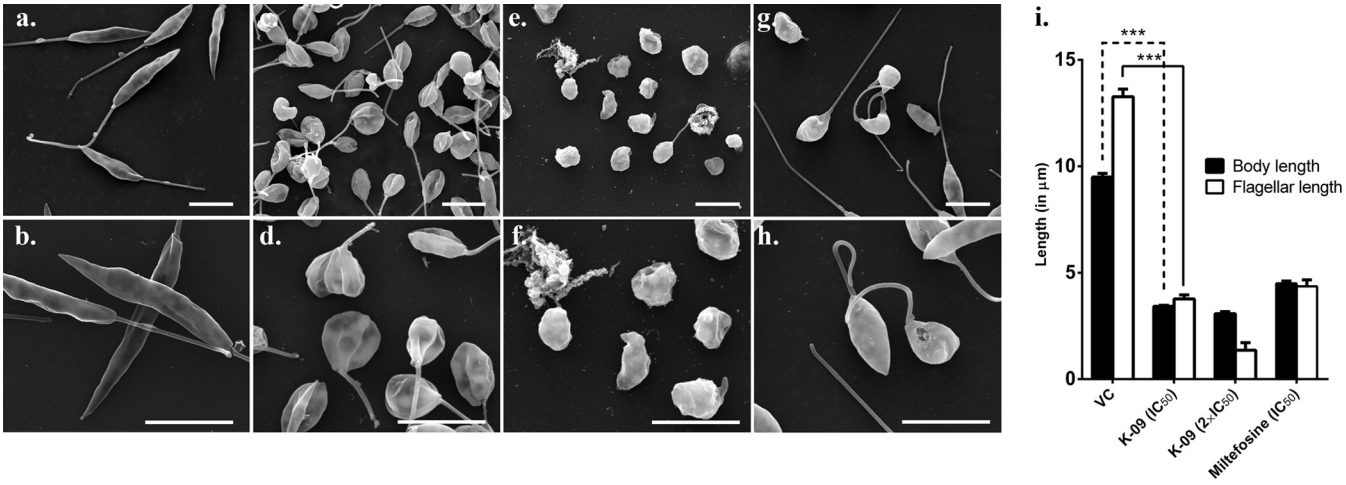

FIG 1 SEM micrographs showing altered morphology of *L. donovani* promastigotes in K-09-treated (c to f) and miltefosine-treated (g and h) cells compared to that of VC (a and b). Note the round cell bodies, shortened flagella (c to f), and presence of membrane folds (c and d) compared to the slender body with long flagella in the VC cells (a and b). (i) Mean body and flagellar length in VC and K-09 (IC_{50} and 2× the IC_{50})-treated parasites. Bars, 5 μm. ***, $P < 0.05$.

stock was added to the samples, which were then incubated on ice for 15 min and finally analyzed by flow cytometry.

Detection of DNA fragmentation by TUNEL assay. Cell death pathways involve the activation of different endonucleases, which cleave genomic DNA into oligonucleosomal fragments of 180 to 200 bp (18). A terminal deoxynucleotidyltransferase-mediated dUTP-biotin nick end labeling (TUNEL) assay works by attaching fluorescein-conjugated dUTP at the 3′ end of nicked DNA by the enzyme terminal deoxynucleotidyl transferase (TdTase). The experiment was performed according to the manufacturer's protocol (DeadEnd fluorometric TUNEL system; Promega, Madison, WI, USA). The cells were harvested, adhered to coverslips, fixed with 4% PFA, and subsequently permeabilized with 0.2% Triton X-100. After equilibrating the cells with TdT equilibration buffer, they were incubated in the recombinant TDT (rTdT) reaction mixture containing equilibration buffer, nucleotide mixture, and rTdT enzyme for 60 min at 37°C. After incubation, the cells were washed once with 2× SSC (1× SSC is 0.15 M NaCl plus 0.015 M sodium citrate), counterstained with 10 μg/ml PI, and visualized under a confocal microscope. Another set of samples was incubated in a suspension in microcentrifuge tubes, according to the same protocol as for confocal imaging, and was analyzed by flow cytometry with a standard fluorescein/phosphatidylethanolamine (PE) filter set.

Statistical calculations. All experiments were performed in triplicate. The values stated are the means ± standard errors of means. Statistically significant differences for the values for two groups were calculated with unpaired Student's *t* test, with differences being significant at a *P* value of <0.05. All calculations of fluorescence intensity were performed on ≥20 cells in the field(s) that displayed fluorescent signals. The values, unless stated otherwise, are the means from three or more similar experiments.

RESULTS

K-09 induces morphological alterations in *L. donovani* promastigotes. Scanning electron microscopy (SEM) was employed to assess morphological alterations in the *Leishmania* promastigotes induced by K-09. SEM analysis of the control cells revealed healthy parasites with typical slender bodies, long flagella, and smooth cell surfaces. At the IC_{50}, K-09-treated cells revealed striking morphological alterations. The cells had shrunk in volume and assumed a round bag-like swollen appearance (Fig. 1c to f), with stumpy flagella. The cell surface showed wrinkling, and multiseptations were observed along the length of the cell (Fig. 1d). Such septations were not observed for miltefosine (a standard antileishmanial drug)-treated cells. At 2× the IC_{50}, the cells were in the late stage of cell death, and SEM micrographs showed that most cells were distorted, lost their flagella completely, and some of them lysed (Fig. 1e and f). A comparative quantitative morphological analysis from the SEM data is shown in Fig. 1i.

K-09 induces gross ultrastructural alterations typical of apoptosis. The subcellular alterations of the parasites induced by K-09 were analyzed by a transmission electron microscopy (TEM) thin-sectioning technique. Normal ultrastructure was observed in control promastigotes. The cells were slender and elongated with kinetoplast containing highly condensed DNA. The VC cells exhibited a single ramified mitochondrion containing well-defined cristae and an electron-dense matrix that extended throughout the length of the parasite (Fig. 2i). The nucleus contained evenly distributed chromatin. Cells treated at the IC_{50} exhibited several ultrastructural distortions typical of apoptotic cells. A reduction in the size of the cells from the slender elongated morphology was observed. The cytoplasm appeared less electron dense, with increased cytoplasmic vacuolation, increased accumulation of lipid droplets, and multivesicular bodies (Fig. 2e and f). Significant swelling and the disruption of the kinetoplast-mitochondrial complex were noticed with decondensation of the kinetoplast (kDNA). Displacement of the kinetoplast and flagellar pocket disruption were also common features noticed in the treated parasites (Fig. 2h). The affected mitochondria showed considerable swelling, with disorganized cristae and a loss in matrix density (Fig. 2j). A considerable amount of pyknosis in the nuclei was observed, while the plasma membrane remained intact.

K-09 depolarizes the mitochondrion, triggering release of cytochrome *c* into the cytosol. Considering the TEM observations on the disruptive effect of K-09 on the mitochondria of the parasites, we next assessed its effect on $\Delta\Psi_m$ using JC-1 staining. Confocal microscopy was used to visualize depolarization, along with flow cytometry and fluorescence spectrophotometry to quantitate $\Delta\Psi_m$. Microscopic observations (Fig. 3b) revealed that cells treated with the IC_{50} of K-09 exhibited significantly greater fluorescence in the green region, indicating a lower $\Delta\Psi_m$, than VC

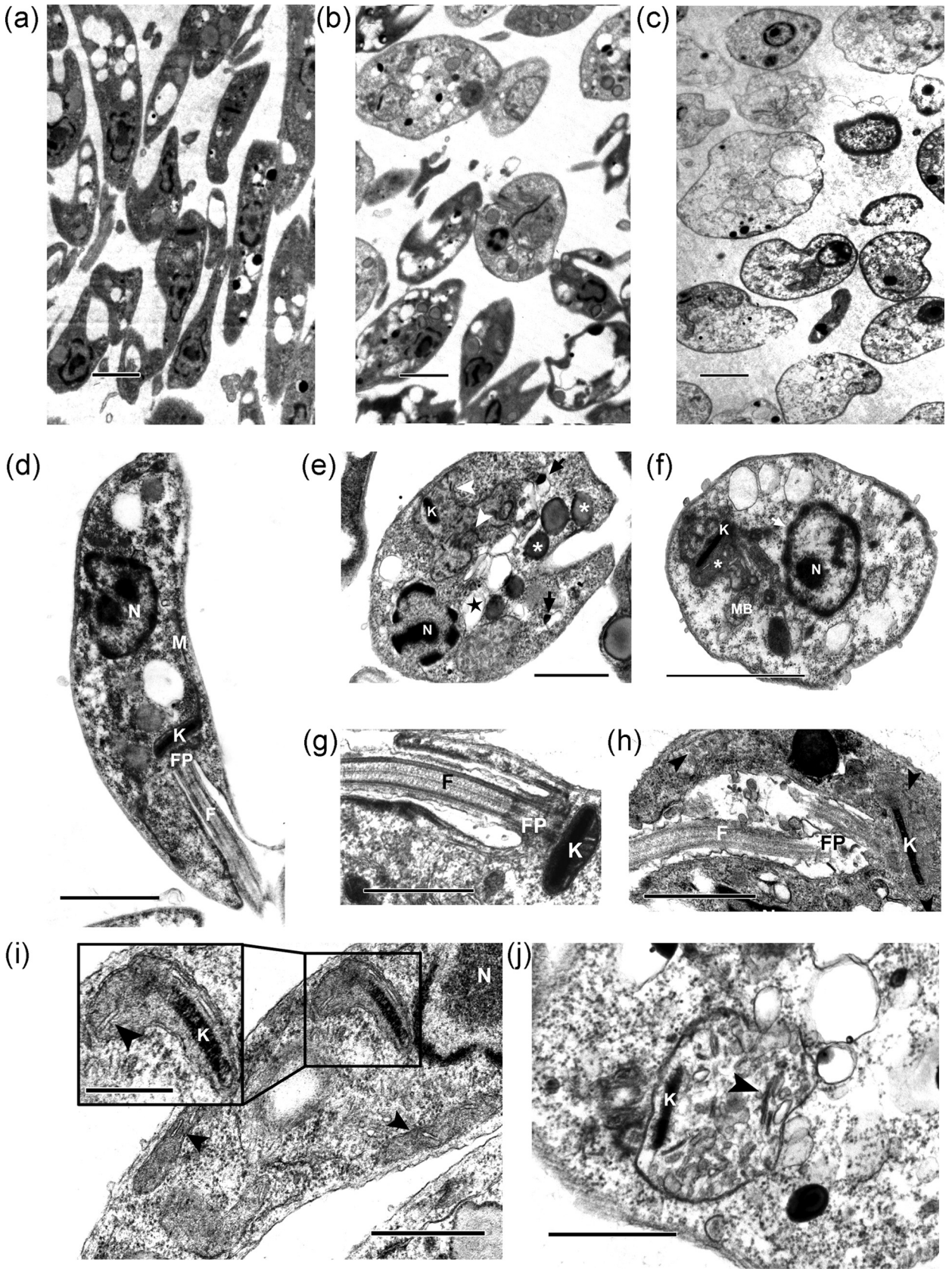

FIG 2 Ultrastructural alterations following K-09 administration in *L. donovani* promastigotes. The cells treated with IC_{50} (b, e, and h) and 2× the IC_{50} (f and j) doses of K-09 show dramatic alterations in the ultrastructure compared to that of the VC cells (a, d, g, and i). Note the change in overall morphology, nuclear condensation (e), distortion of the flagellar pocket (h), appearance of lipid reservoirs (e, asterisk) and multilamellar bodies (MB) (f), fragmentation of the mitochondrion (e and h, arrowheads), and the disruption of the mitochondria-kinetoplast complex (f, asterisk) with disorganized cristae (j, arrowhead) against VC cells (i, inset). Also note the increase in vacuoles (e, star) and acidocalcisomes (e, black arrows). N, nucleus; K, kinetoplast; F, flagellum; FP, flagellar pocket; M, mitochondrion. Bars, 1 μm (a to f), 500 nm (g to j), and 250 nm (inset).

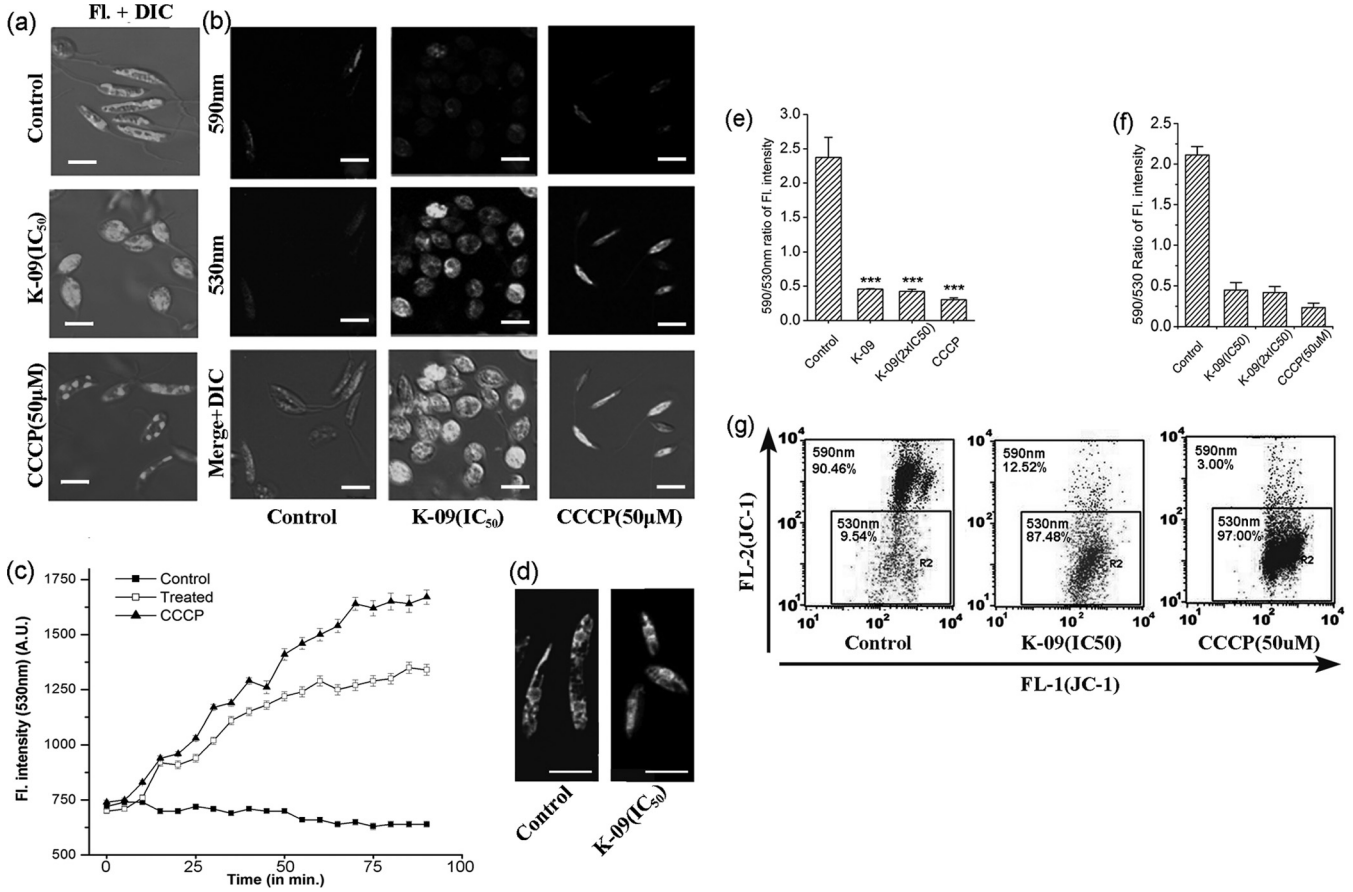

FIG 3 Depolarization of the *L. donovani* mitochondrion and release of cytochrome *c* into the cytosol following K-09 treatment. (a) Pattern of mitochondrial distribution along the cell before and after treatment with K-09 and CCCP. Note that the ramified mitochondrial network present in the VC cells is disrupted upon K-09 and CCCP treatment. (b) Confocal imaging of cells treated with K-09 and stained with JC-1, showing increased fluorescence in the green channel, indicating depolarized mitochondria. (c) Gradual mitochondrial depolarization in cells treated with K-09 and CCCP, and stained with JC-1 showing sharp fall in $\Delta\Psi_m$, indicated by increasing JC-1 fluorescence in green channel. (d) Confocal images of VC and cells treated with K-09 and that were stained for cytochrome *c* localization. Note the same ramified pattern of mitochondrion as in panel a in the VC, as well as the diffused cytosolic staining in the treated cells, indicating cytochrome *c* release from the mitochondria. (e) Ratio of fluorescence (red/green channel) from panel b, showing $\Delta\Psi_m$ loss upon K-09 treatment. (f) Ratio of fluorescence intensity in red/green channel after 24 h of treatment. (g) Flow cytometric analysis of K-09- and CCCP-treated cells showing similar results. Bars, 5 μm. ***, $P < 0.001$. A.U., arbitrary units; Fl., fluorescence; DIC, differential interference contrast.

cells that exhibited mitochondrial fluorescence in the red region, indicating a higher $\Delta\Psi_m$. K-09 treatment resulted in an ~5-fold decrease in the JC-1 fluorescence intensity ratio (red/green). A similar response was observed in CCCP-treated cells, indicating depolarization of the mitochondrial membrane. Gradual mitochondrial depolarization by K-09 was also monitored by kinetic fluorometric measurements at 530 nm (Fig. 3c). Treatment with 2× the IC_{50} of K-09 resulted in an ~2-fold increase in fluorescence intensity over the VC cells after 90 min. Flow cytometry analysis of the K-09-treated cells at the IC_{50} and 2× the IC_{50} for 24 h showed 87.5% and 97% depolarized mitochondria, respectively, compared to 9.5% VC (Fig. 3g). The translocation of cytochrome *c* from the mitochondria into the cytosol after K-09 treatment was confirmed by immunofluorescence microscopy (Fig. 3d).

K-09 treatment impairs ATP production. Since intracellular ATP content is a direct marker of the energy state and thus the health of the mitochondrion of the cell, we measured ATP content using a bioluminescence assay. K-09 treatment resulted in a marked reduction in the ATP levels in promastigotes and intracellular amastigotes. The total ATP contents of the promastigotes treated with the IC_{50} and 2× the IC_{50} of K-09 were 4.2- and 4.8-fold lower than those of the VC (Fig. 4a). The addition of oli-A after 2 h of IC_{50} K-09 exposure in low-glucose (LG) (containing 1 mg/ml glucose) and glucose-free medium caused severe depletion of the cellular ATP content. However, oli-A did not significantly prevent ATP depletion of K-09-treated cells in the presence of high glucose (glycolytic substrate) (Fig. 4b) and also did not rescue K-09-treated cells from cell death (Fig. 4c). In the intracellular amastigotes, we observed that the addition of oli-A (in LG medium) following K-09 treatment caused a 4.2-fold drop in the cellular ATP pool of the infected macrophages and an 8.4-fold drop in the presence of HG medium compared with the same events in infected macrophages treated with K-09 alone in HG medium (Fig. 4d).

K-09-induced mitochondrial depolarization generates ROS and causes oxidative stress. Confocal microscopy of the cells stained with the ROS probe carboxy-H_2DCFDA revealed that majority of the cells treated with the IC_{50} of K-09 fluoresced evenly throughout the cells, while no fluorescence was observed in the VC cells, indicating elevated ROS levels posttreatment (Fig. 5a).

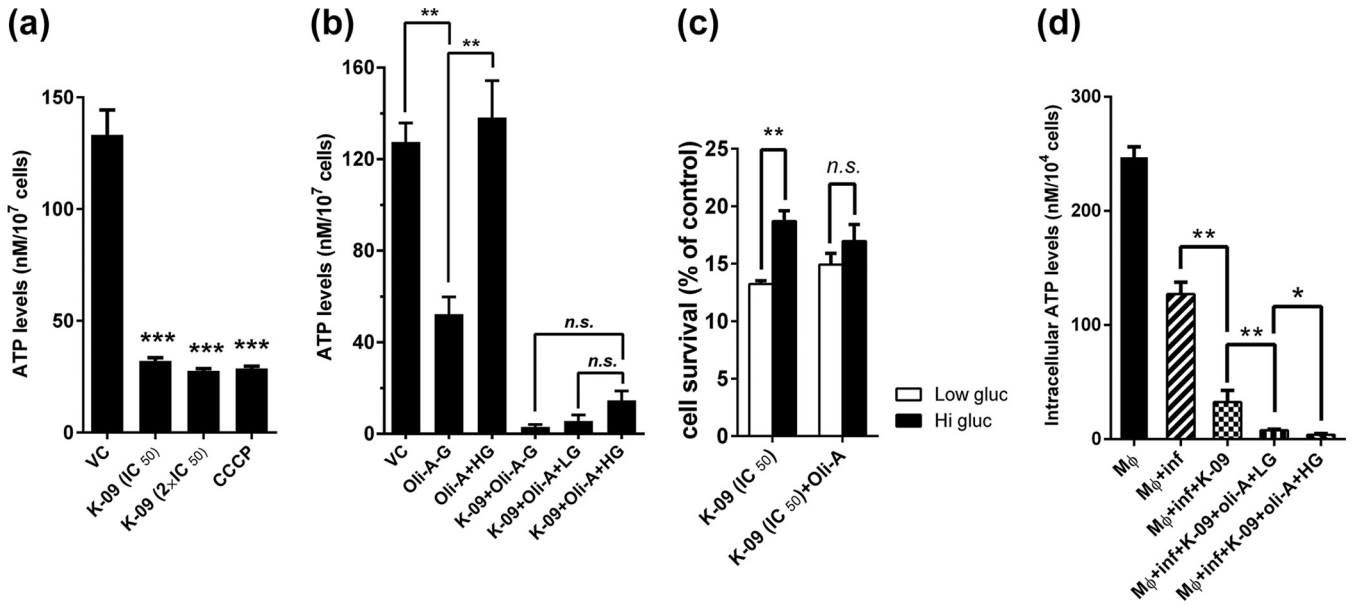

FIG 4 Depletion of cellular ATP pool in *L. donovani* promastigotes and amastigotes after K-09 treatment. (a) Intracellular ATP levels decrease with K-09 and CCCP treatment. (b) Addition of oli-A in the presence of glucose prevented ATP depletion in promastigotes but not in the case of the K-09-treated cells. (c) Survival of promastigotes was not significantly altered with the addition of oli-A in K-09-treated cells in low-glucose (low gluc) or high-glucose (hi gluc) medium. (d) K-09 also induced ATP depletion in amastigotes, which was moderately reduced by the addition of oli-A in the presence of either low or high glucose. Mϕ, macrophages; Mϕ+inf, infected macrophages; HG, high glucose; LG, low glucose; −G, no glucose. *, $P < 0.05$; **, $P < 0.01$; ***, $P < 0.001$; *n.s.* (nonsignificant), $P > 0.05$.

Similar results were obtained with TBHP, a positive control. The cells pretreated with NAC showed fluorescence comparable to that of the VC cells. After 24 h, K-09 treatment showed a 2.5-fold increase in ROS levels compared to those of the VC (Fig. 5d), while NAC pretreatment maintained ROS levels almost on par with those of the VC. The cell-permeable fluorogenic probe MitoSOX red was used as a mitochondrial superoxide probe and visualized by confocal microscopy. The control cells exhibited weak fluorescence, whereas the K-09-treated cells exhibited intense red fluorescence, indicative of severe oxidative stress (Fig. 5b and c). To confirm whether mitochondrial depolarization precedes ROS generation, we performed time-lapse fluorometric experiments after pretreating cells with NAC and exposing them to K-09. A steady increase in cytosolic calcium (using Fluo-4 AM) and mitochondrial depolarization was observed, but no increase in the intracellular ROS level was detectable (Fig. 5f to h).

K-09-induced oxidative stress causes GSH depletion. Cells have developed the cellular thiol buffer system to neutralize free radical damage, and its principal component, GSH (reduced glutathione), is an important free radical scavenger that works by donating an electron to ROS, thereby forming GSSG (oxidized glutathione) and thus aiding the survival of the cell (9, 19). Cellular GSH levels in treated and NAC-pretreated cells were monitored with MCB dye. We observed that NAC pretreatment led to an increase in the GSH content of the cells over that of the VC by salvaging free radicals, whereas treatment with the IC_{50} and 2× the IC_{50} of K-09 depleted the cellular GSH levels by 45% and 33%, respectively (Fig. 5e).

K-09 treatment results in elevation of cytosolic calcium levels. Since the disruption of calcium homeostasis by its release from intracellular stores, like the endoplasmic reticulum (ER) and acidocalcisomes, is a critical event triggered by chemotherapeutic agents (13, 20), we explored the effect of K-09 on the intracellular Ca^{2+} level using the dye Fluo-4 AM, which has been used to measure intracellular calcium (15). We observed a prompt rise in Fluo-4 AM fluorescence within 5 min of adding 2× the IC_{50} of K-09, which steadily increased following K-09 treatment up to 1.5 h, after which it saturated to a plateau. At this point, an ~2-fold increase in fluorescence against the VC was observed (Fig. 6b). Ionomycin, a Ca^{2+} ionophore, rendered greater than twice the fluorescence intensity of the VC cells after 1.5 h, while cells exposed to the drug in the presence of Ca^{2+} chelator EGTA in the medium showed fluorescence similar to that of VC, indicating that most of the calcium responsible for fluorescence increase is extracellular (Fig. 6c). These results are corroborated by confocal microscopy findings (Fig. 6a).

K-09 induces sub-G_0/G_1 phase cell cycle arrest in *L. donovani* promastigotes. The DNA content analysis of untreated promastigote populations showed negligible cells in the sub-G_0/G_1 region, while cells treated with the IC_{50} of K-09 showed about 57% of the cells to be apoptotic in the sub-G_0/G_1 region, and cells treated with 2× the IC_{50} of K-09 showed 93% of the cells to be in the apoptotic fraction (Fig. 7).

K-09 triggers phosphatidylserine reversal. The externalization of phosphatidylserine (PS) was visualized using annexin V-FITC staining. We observed that the cells treated with the IC_{50} of K-09 displayed bright FITC fluorescence along their periphery, indicating PS externalization and induction of apoptosis (Fig. 8a). In contrast, pretreatment with the caspase-3/-7 inhibitor Ac-DEVD-CHO led to the inhibition of PS externalization after K-09 treatment.

Involvement of caspase-like proteases in K-09-induced apoptosis. To confirm caspase-like protease activity in K-09-mediated apoptosis, we employed confocal imaging of a caspase-

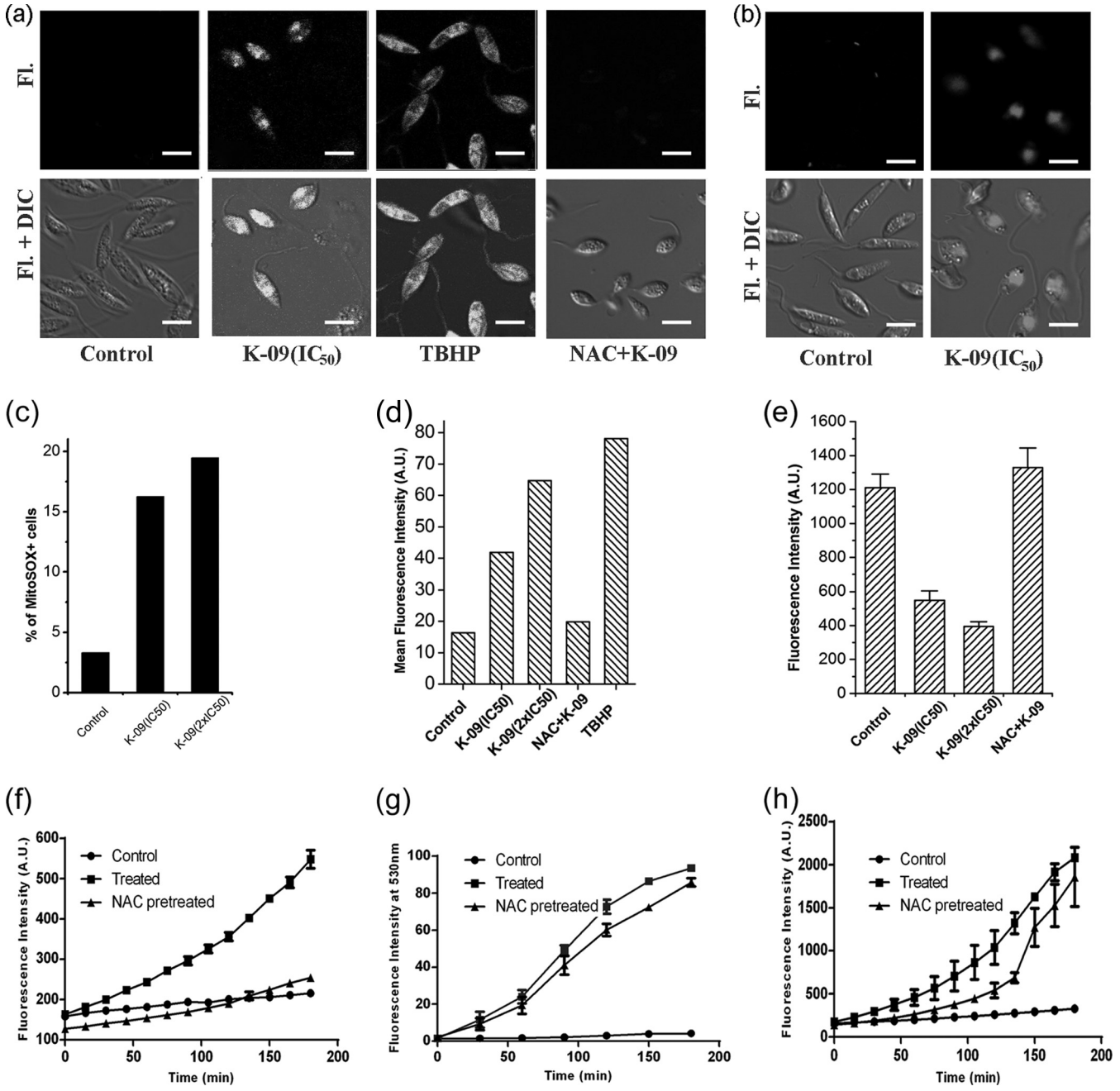

FIG 5 K-09 generates reactive oxygen species (ROS) and promotes oxidative stress. (a) Reactive oxygen species levels visualized with carboxy-H_2DCFDA and analyzed by confocal microscopy. Note that NAC prevents an increase of ROS levels. (b) Confocal micrograph of cells stained with MitoSOX red. (c) Percentage of cells showing MitoSOX red fluorescence, analyzed by flow cytometry. (d) Carboxy-H_2DCFDA fluorescence after 24 h of K-09 treatment. (e) Cellular reduced glutathione levels (stained with MDC) after 24 h of treatment. Error bars indicate standard errors of the means. Monitoring changes in intracellular ROS (f), mitochondrial membrane potential (g), and Ca^{2+} levels (h) when cells were pretreated with 20 mM NAC (for 2 h). Bars, 5 μm.

specific fluorescent substrate (NucView 488; Biotium). We observed distinct fluorescence inside the nuclei of the K-09-treated cells, a characteristic of this dye, where the caspase-cleaved fluorescent product binds to DNA. Such fluorescence was totally absent in the VC cells. Pretreatment with Ac-DEVD-CHO before drug treatment prevented any fluorescence in the nuclear region (Fig. 8b).

DNA fragmentation on K-09 exposure. To investigate the induction of DNA fragmentation on K-09 exposure, a TUNEL assay was performed. The samples were analyzed by flow cytometry and revealed approximately 4% TUNEL-positive ($TUNEL^+$) cells in the untreated promastigotes and 58% and 86% $TUNEL^+$ cells in the cells treated with IC_{50} and 2× the IC_{50} doses of K-09, respectively, after 24 h of drug treatment (Fig. 8c).

K-09 treatment alters lipid metabolism in *L. donovani* promastigotes. Since TEM analysis revealed an increased number of

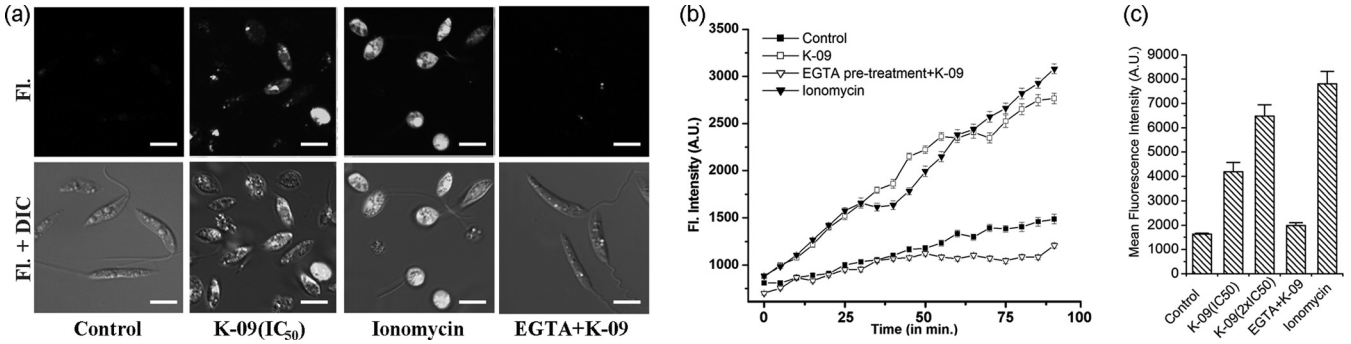

FIG 6 Increment of intracellular Ca^{2+} levels following K-09 administration. (a) Cells stained with the Ca^{2+} sensor dye Fluo-4 AM and analyzed by confocal microscopy. Note that the presence of the Ca^{2+} chelator EGTA during K-09 treatment abrogates the rise of Ca^{2+} levels. (b) Intracellular Ca^{2+} levels following K-09 administration monitored up to 90 min. (c) Fluo-4 AM fluorescence after 24-h treatment with K-09 measured using a fluorometer. Error bars indicate standard errors of the means.

lipid droplets after K-09 treatment, we confirmed this observation with Nile red staining of live parasites. A significant increase in the number of cytoplasmic lipid droplets at the IC_{50} of K-09 (Fig. 8d and e) was observed. However, at 2× the IC_{50} of K-09, the smaller droplets probably fused to form larger ones, represented by a corresponding decrease in the mean droplet count.

DISCUSSION

The promising antileishmanial agent K-09 was recently reported to be safe and orally active in a hamster model for VL (11). This clerodane diterpene was shown to be a DNA topoisomerase inhibitor using biochemical assays and molecular docking studies (11). The detailed mode of action of this agent, however, has remained uncharacterized. Therefore, in the present study, we have investigated the physiological and ultrastructural effects of K-09 on *L. donovani* promastigotes to further dissect the mechanism of cell death induction that is used by this compound.

Morphological alterations in *L. donovani* promastigotes induced by K-09 were studied using electron microscopy, which remains the gold standard for diagnosing the nature of cell death (21). Since the genus *Leishmania* diverged early in the evolution from the metazoans, there are significant differences in cell death at the molecular level in this unicellular organism. This makes it difficult to interpret results when commonly used metazoan apoptotic biomarkers are used in cell death assays. Unicellular kinetoplastid parasites have special organelles involved in essential metabolic pathways, with steps differing from their mammalian counterparts, thus making them attractive targets for new chemotherapeutic agents. Here, ultrastructural studies can be very helpful in achieving this goal (22). Our SEM observations revealed swelling and overall rounding up of K-09-treated cells, with a significant loss in body length and shortening of flagella compared to the untreated cells. One notable finding was the presence of distinct membrane folds in the K-09-treated cells. This feature was not observed in the miltefosine-treated cells. Similar observations have also been reported in promastigotes upon treatment with geldanamycin and cyclosporine (23, 24), in which the molecular chaperone Hsp90 inactivation has been implicated. Most likely, K-09 also directly or indirectly inhibits Hsp90 to trigger such topological alterations. TEM observations revealed that K-09 treatment resulted in the morphological features typical of apoptosis. Subcellular alterations included the rounding up of cells, intense cytoplasmic vacuolation, pyknosis of the nucleus, structural disruption of the mitochondrion, and decondensation of the kinetoplast. Previous studies have described similar observations of mitochondrion-kinetoplast damage upon treatment in *Leishmania*

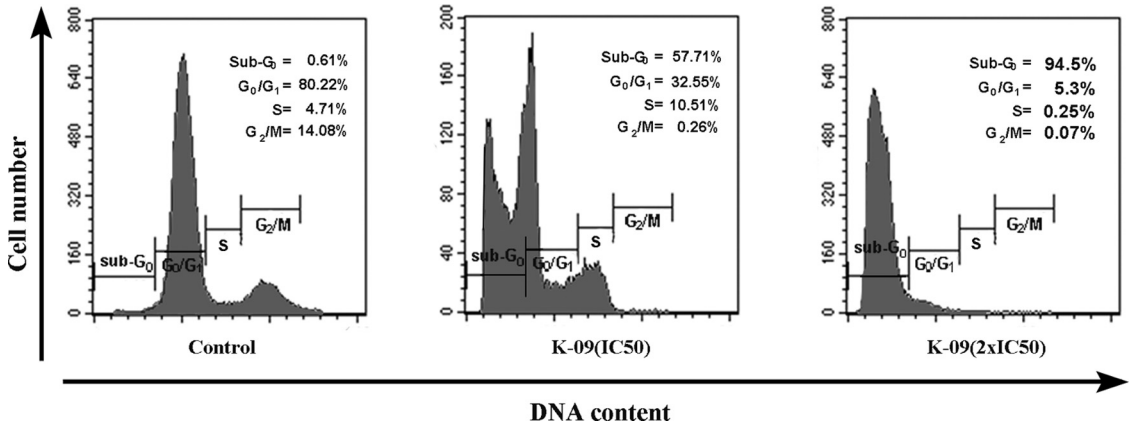

FIG 7 Cell cycle arrest in *L. donovani* promastigotes with K-09 treatment. A DNA content analysis after 24 h of drug treatment was performed after PI staining using flow cytometry. Note the normal cell cycle profile of the VC cells while K-09 treatment arrests cells in the sub-G_0/G_1 phase in proportion to the dose of IC_{50} and 2× the IC_{50} of K-09.

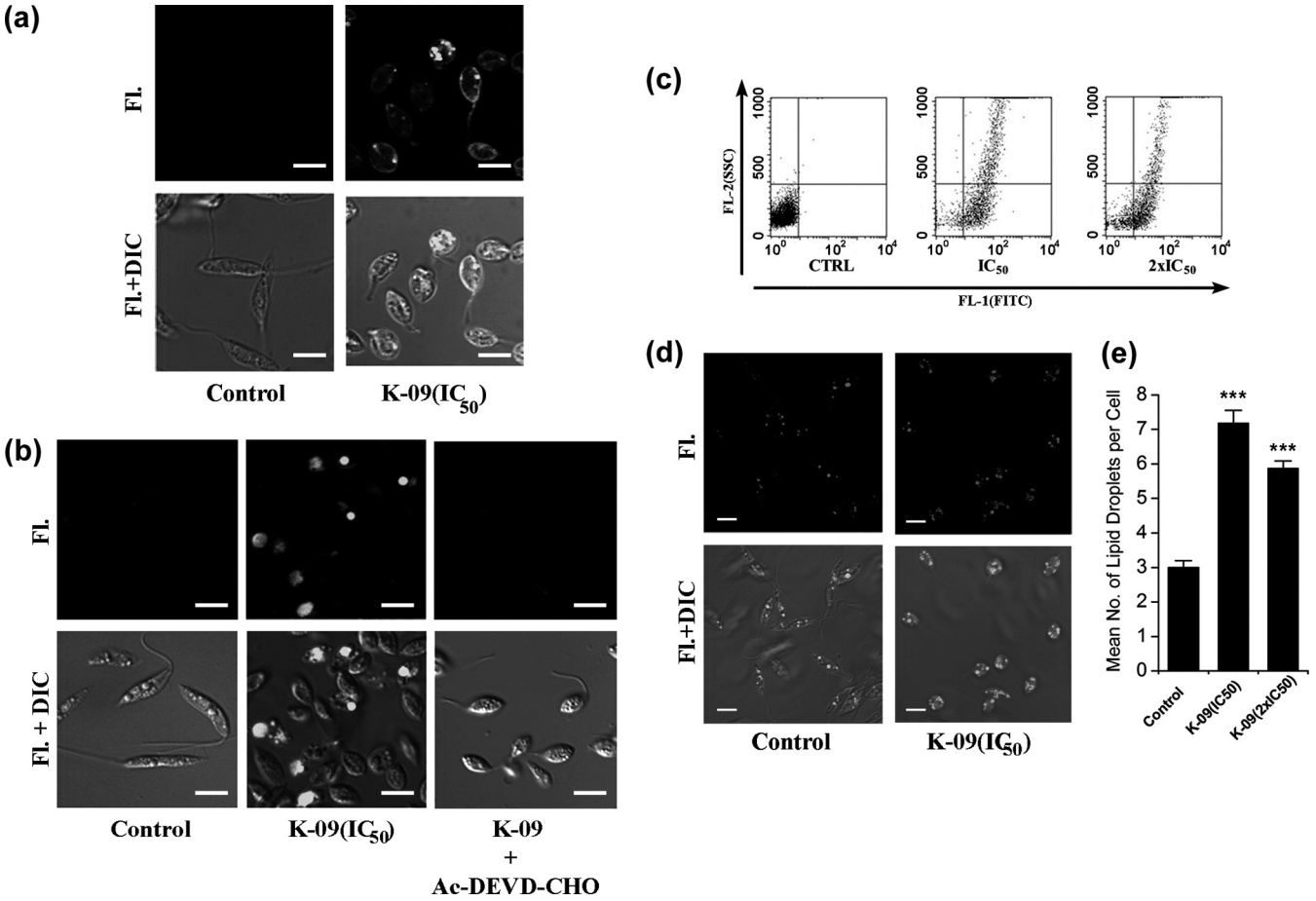

FIG 8 Apoptotic markers in K-09-treated parasites. (a) Annexin V-FITC-stained cells with and without IC_{50} K-09 treatment. The VC cells show no annexin V-FITC fluorescence, while the K-09-treated cells show annular fluorescence along the cell periphery, suggesting a reversal of PS. The cells pretreated with the caspase-3/-7 inhibitor Ac-DEVD-CHO show a decrease in fluorescence, implying that apoptosis has been prevented. (b) Caspase-3/-7-like protease activity present in apoptosis following K-09 treatment, which is abrogated by Ac-DEVD-CHO. (c) Flow cytometric analysis of $TUNEL^+$ cells after K-09 (IC_{50} and 2× the IC_{50}) treatment. Also shown are the confocal imaging (d) and quantification of the number of lipid droplets (e) after K-09 treatment (single-plane image). Bars, 5 μm. ***, $P < 0.001$.

amazonensis promastigotes with a putrescine analogue (25), the antiarrhythmic drug amiodarone (20), and a squalene synthase inhibitor, BPQ-OH (26).

Since the mitochondrion plays a pivotal role in orchestrating apoptosis, and *Leishmania* parasites possess only one large ramified mitochondrion that caters to the majority of their energy requirements (27), irreversible damage and dysfunction of this vital organelle would have disastrous consequences on their survival. Thus, these observations have serious implications for the design of drugs against this parasite. The disruption of the structural integrity of the mitochondria through damage to its inner membrane might also account for the decondensation of the kinetoplast, since the inner membrane holds the kinetoplast (28). Membrane blebbing, a common feature in metazoan apoptosis, was notably absent, which is not surprising, since this unicellular eukaryote has a different set of molecular players controlling apoptosis compared to that of metazoans. Alterations in the flagellar pocket region without major plasma membrane disruption at the IC_{50} dose was another major piece of evidence suggesting the disruption of microtubule dynamics, leading to the inhibition of intracellular trafficking of nutrients by K-09, since endocytosis and exocytosis are the central processes that take place in this cellular region (12, 29).

Although TEM micrographs identified the mitochondrion as the organelle that is severely affected upon K-09 exposure, the underlying mechanism of action remained elusive. Thus, we investigated whether K-09 affected mitochondrial membrane potential and processes driven by it, such as ATP production, especially since the parasite depends mainly on oxidative phosphorylation for ATP production (27). Our observations point out that K-09 depolarized the parasite mitochondria and impaired ATP production. We also sought to understand whether oligomycin-A (an inhibitor of the mitochondrial F_oF_1 ATP synthase), which is known to prevent ATP depletion and rescue procyclic *Trypanosoma brucei* cells from death under glucose-rich conditions, could do the same in K-09-treated *L. donovani*. Oli-A treatment alone prevented ATP depletion in the presence of high glucose compared to that in glucose-free medium but not in K-09-treated cells. This observation is in agreement with previous studies that report the existence of an energy-compensatory mechanism in the form of substrate-level phosphorylation that is activated in the procyclic form of *T. brucei* under conditions that

favor glycolysis or when oxidative phosphorylation is under stress by agents, such as oli-A (30). Additionally, oli-A in HG medium after K-09 exposure did not rescue cells compared with oli-A in LG medium without K-09 exposure. A possible explanation is that mitochondrial depolarization, a so-called point of no return of cell death, may be an event that is upstream of ATP depletion in K-09-induced apoptosis, and cells with depolarized mitochondria may be irreversibly committed to the cell death pathway. The release of the proapoptotic protein cytochrome *c*, an essential component of the electron transport chain that localizes in the mitochondria, into the cytosol of the parasite upon mitochondrial dysfunction is another characteristic feature of PCD in kinetoplastids (17, 31). The release of cytochrome *c* into the cytosol after K-09 treatment suggests the opening of MPTP to be another important event initiated by this diterpene.

While mitochondrial depolarization and cytochrome *c* release are critical, it is the subsequent elevation in the levels of oxidizing species generated from the mitochondria that plays the role of cytotoxic effectors in apoptosis. In *Leishmania* organisms, as in other metazoans, there is a basal level of ROS maintained by the mitochondria inside the cells for physiological signaling (32). The onset of mitochondrial dysfunction due to the disruption of its structural integrity causes leakage in the electron transport chain (ETC) and thus elevates ROS levels. Reports of antitrypanosomal activity for mitochondrial disruptors include 3,3′-diindolylmethane (15), tafenoquine (33), and sitamaquine (34), which inhibit F_oF_1 ATP synthase, complex III, and complex II of the parasite mitochondrion, respectively. Antileishmanial agents, such as baicalein (31) and amiodarone (20), induce oxidative stress and cytosolic calcium increase, respectively, which then depolarizes mitochondria to generate ROS. Elevated ROS levels are buffered by the cellular GSH pool, which causes its depletion (15, 35). Dose-dependent depletion of the cellular GSH pool and an increase in the ROS levels upon K-09 exposure were observed, while pretreatment with NAC maintained the GSH pool and ROS levels on par with those of VC cells. NAC pretreatment prior to K-09 exposure, however, was unable to prevent mitochondrial depolarization and a rise in intracellular calcium. This demonstrates that intracellular ROS generation occurs downstream of mitochondrial depolarization and intracellular calcium rise.

The disruption of intracellular calcium homeostasis is another characteristic feature of PCD in *Leishmania*. Several studies have reported mitochondrial depolarization and subsequent ROS generation to be intimately associated with the dysregulation of intracellular calcium homeostasis (8, 13, 20, 31). K-09 treatment results in an elevation in cytoplasmic calcium, possibly due to the influx of Ca^{2+} from the extracellular medium through the activation of plasma membrane Ca^{2+}-ATPase (PMCA).

K-09 treatment also resulted in an increase in the number of lipid droplets inside the promastigote, which was observed by TEM analysis and NR staining. Similar observations have been reported in *L. amazonensis* after treatment with squalene synthase inhibitors and amiodarone (20, 29). These observations were attributed to the inhibition of sterol biosynthesis in the parasite, causing formation of lipid bodies composed of abnormal intermediate metabolites (29). Interestingly, previous studies have implicated this diterpene as an inhibitor of 3-hydroxy-3-methylglutaryl–coenzyme A (HMG-CoA) reductase (HMGR) (36), a rate-limiting enzyme present in the mitochondria of trypanosomatids and that is required for the synthesis of ergosterols (37). Also, a study on the regulation of HMGR of *Leishmania major* reported that the enzyme has higher affinity for lovastatin, its competitive inhibitor, than for its natural substrate HMG-CoA. In another study, however, incubation with lovastatin activated increased HMGR activity in the promastigotes (38). It is probable that the rise in the number of lipid droplets observed with K-09 treatment might be due to the hyperactivity of HMGR, as K-09 was shown to be a structural analogue of lovastatin (36). This presumably leads to the overproduction of the lipid precursors that accumulate in the form of lipid droplets.

It is well-known that caspases, a family of cysteine proteases, are involved in orchestrating apoptosis in metazoans. Caspase homologues known as metacaspases in *Trypanosoma* and *Leishmania* have been reported to play distinct roles in PCD (39, 40), though their caspase-substrate cleaving has activities have been debated, as has the role of the requirement of an active site cysteine in the substrate (40). However, the *L. donovani* caspase homologues *Ld*MC1 and *Ld*MC2 have been shown to be essential in cell cycle proliferation (41). Studies have detected a significantly larger amount of active-form metacaspase in cells undergoing H_2O_2-induced PCD (8), as well as elevated metacaspase gene expression in miltefosine-induced PCD (42). However, studies that report caspase-independent PCD in these parasites might suggest that metacaspase involvement is not essential (13, 34). In our study, we found major upregulation of caspase-3/-7-like protease levels in cells following K-09 exposure, and the pretreatment of cells with the caspase-3 inhibitor Ac-DEVD-CHO diminished caspase-3/-7-like protease activity and PS externalization.

After its identification and first report from *P. longifolia* in 1988 (43), K-09 has been reported to show diverse pharmacological activities, such as antimalarial (44), antimicrobial, and antidyslipidemic (36, 45) activities, before recently being reported as an antileishmanial agent by topoisomerase I inhibition (11). In summary, we have shown that K-09 induces PCD in *L. donovani* promastigotes by mitochondrial dysfunction, causing an elevation of ROS to cytotoxic levels inside the cells, which mediates cell death in a caspase-like protease-dependent manner. Our study adds to the growing body of evidence that there is an apoptosis-like PCD mechanism in these unicellular protists similar to that of metazoan PCD. The identification and characterization of the molecular players involved at different checkpoints can be useful in discovering and screening for potential molecular targets for rational drug design. In conclusion, our work provides a basis for further investigation of the development of K-09 as a potential drug candidate for VL.

ACKNOWLEDGMENTS

We thank A.A. Sahasrabuddhe for his support and access to his cell culture laboratory during the initial stages of the study and also for sharing *L. donovani* strain MHOM/IN/80/DD8. We also thank A.L. Vishwakarma for flow cytometry analysis and K. Singh and M. Srivastava for technical assistance during TEM sample preparation. We thank N. Goyal for sharing the J774.A1 macrophage cell line and R.S. Bhatta and D.P. Mishra for access to fluorescence spectrophotometers. We are grateful to the Director of CSIR-CDRI for providing facilities and infrastructure for this study.

This is CDRI communication no. 8747.

Funding was provided by the Council of Scientific and Industrial Research (CSIR) network project BSC0114. M.K. and A.B. are recipients of CSIR JRF.

We declare no conflicts of interests.

REFERENCES

1. **Myler PJ, Fasel N (ed).** 2008. *Leishmania*: after the genome. Caister Academic Press, Portland, OR.
2. **Mishra J, Saxena A, Singh S.** 2007. Chemotherapy of leishmaniasis: past, present and future. Curr. Med. Chem. **14:**1153–1169. http://dx.doi.org/10.2174/092986707780362862.
3. **Croft SL, Sundar S, Fairlamb AH.** 2006. Drug resistance in leishmaniasis. Clin. Microbiol. Rev. **19:**111–126. http://dx.doi.org/10.1128/CMR.19.1.111-126.2006.
4. **Tagboto S, Townson S.** 2001. Antiparasitic properties of medicinal plants and other naturally occurring products. Adv. Parasitol. **50:**199–295. http://dx.doi.org/10.1016/S0065-308X(01)50032-9.
5. **Kaczanowski S, Sajid M, Reece SE.** 2011. Evolution of apoptosis-like programmed cell death in unicellular protozoan parasites. Parasit. Vectors **25:**4–44. http://dx.doi.org/10.1186/1756-3305-4-44.
6. **Lee N, Bertholet S, Debrabant A, Muller J, Duncan R, Nakhasi HL.** 2002. Programmed cell death in the unicellular protozoan parasite *Leishmania*. Cell Death Differ. **1:**53–64. http://dx.doi.org/10.1038/sj/cdd/4400952.
7. **Raina P, Kaur S.** 2006. Chronic heat-shock treatment driven differentiation induces apoptosis in *Leishmania donovani*. Mol. Cell. Biochem. **289:**83–90. http://dx.doi.org/10.1007/s11010-006-9151-5.
8. **Das M, Mukherjee SB, Shaha C.** 2001. Hydrogen peroxide induces apoptosis-like death in *Leishmania donovani* promastigotes. J. Cell Sci. **114:**2461–2469.
9. **Sen N, Das BB, Ganguly A, Mukherjee T, Tripathi G, Bandyopadhyay S, Rakshit S, Sen T, Majumder HK.** 2004. Camptothecin induced mitochondrial dysfunction leading to programmed cell death in unicellular hemoflagellate *Leishmania donovani*. Cell Death Differ. **11:**924–936. http://dx.doi.org/10.1038/sj.cdd.4401435.
10. **Paris C, Loiseau PM, Bories C, Bréard J.** 2004. Miltefosine induces apoptosis-like death in *Leishmania donovani* promastigotes. Antimicrob. Agents Chemother. **48:**852–859. http://dx.doi.org/10.1128/AAC.48.3.852-859.2004.
11. **Misra P, Sashidhara KV, Singh SP, Kumar A, Gupta R, Chaudhaery SS, Gupta SS, Majumder HK, Saxena AK, Dube A.** 2010. 16α-Hydroxycleroda-3,13 (14)Z-dien-15,16-olide from *Polyalthia longifolia*: a safe and orally active antileishmanial agent. Br. J. Pharmacol. **159:**1143–1150. http://dx.doi.org/10.1111/j.1476-5381.2009.00609.x.
12. **Katta SS, Tammana TV, Sahasrabuddhe AA, Bajpai VK, Gupta CM.** 2010. Trafficking activity of myosin XXI is required in assembly of *Leishmania* flagellum. J. Cell Sci. **123:**2035–2044. http://dx.doi.org/10.1242/jcs.064725.
13. **Dolai S, Pal S, Yadav RK, Adak S.** 2011. Endoplasmic reticulum stress-induced apoptosis in *Leishmania* through Ca^{2+}-dependent and caspase-independent mechanism. J. Biol. Chem. **286:**13638–13646. http://dx.doi.org/10.1074/jbc.M110.201889.
14. **Kamencic H, Lyon A, Paterson PG, Juurlink BH.** 2000. Monochlorobimane fluorometric method to measure tissue glutathione. Anal. Biochem. **286:**35–37. http://dx.doi.org/10.1006/abio.2000.4765.
15. **Roy A, Ganguly A, BoseDasgupta S, Das BB, Pal C, Jaisankar P, Majumder HK.** 2008. Mitochondria-dependent reactive oxygen species-mediated programmed cell death induced by 3,3′-diindolylmethane through inhibition of F_oF_1-ATP synthase in unicellular protozoan parasite *Leishmania donovani*. Mol. Pharmacol. **74:**1292–1307. http://dx.doi.org/10.1124/mol.108.050161.
16. **Greenspan P, Mayer EP, Fowler SD.** 1985. Nile Red: a selective fluorescent stain for intracellular lipid droplets. J. Cell Biol. **100:**965–973. http://dx.doi.org/10.1083/jcb.100.3.965.
17. **Arnoult D, Akarid K, Grodet A, Petit PX, Estaquier J, Ameisen JC.** 2002. On the evolution of programmed cell death: apoptosis of the unicellular eukaryote *Leishmania major* involves cysteine proteinase activation and mitochondrion permeabilization. Cell Death Differ. **9:**65–81. http://dx.doi.org/10.1038/sj.cdd.4400951.
18. **Zangger H, Mottram JC, Fasel N.** 2002. Cell death in *Leishmania* induced by stress and differentiation: programmed cell death or necrosis? Cell Death Differ. **9:**1126–1139. http://dx.doi.org/10.1038/sj.cdd.4401071.
19. **Davis W, Jr, Ronai Z, Tew KD.** 2001. Cellular thiols and reactive oxygen species in drug-induced apoptosis. J. Pharmacol. Exp. Ther. **296:**1–6.
20. **de Macedo-Silva ST, de Oliveira Silva TLA, Urbina JA, de Souza W, Rodrigues JC.** 2011. Antiproliferative, ultrastructural, and physiological effects of amiodarone on promastigote and amastigote forms of *Leishmania amazonensis*. Mol. Biol. Int. **2011:**876021. http://dx.doi.org/10.4061/2011/876021.
21. **Yasuhara S, Zhu Y, Matsui T, Tipirneni N, Yasuhara Y, Kaneki M, Rosenzweig A, Martyn JA.** 2003. Comparison of comet assay, electron microscopy, and flow cytometry for detection of apoptosis. J. Histochem. Cytochem. **51:**873–885. http://dx.doi.org/10.1177/002215540305100703.
22. **Rodrigues JC, de Souza W.** 2008. Ultrastructural alterations in organelles of parasitic protozoa induced by different classes of metabolic inhibitors. Curr. Pharm. Des. **14:**925–938. http://dx.doi.org/10.2174/138161208784041033.
23. **Wiesgigl M, Clos J.** 2001. Heat shock protein 90 homeostasis controls stage differentiation in *Leishmania donovani*. Mol. Biol. Cell **12:**3307–3316. http://dx.doi.org/10.1091/mbc.12.11.3307.
24. **Yau WL, Blisnick T, Taly JF, Helmer-Citterich M, Schiene-Fischer C, Leclercq O, Li J, Schmidt-Arras D, Morales MA, Notredame C, Romo D, Bastin P, Späth GF.** 2010. Cyclosporin A treatment of *Leishmania donovani* reveals stage-specific functions of cyclophilins in parasite proliferation and viability. PLoS Negl. Trop. Dis. **4:**e729. http://dx.doi.org/10.1371/journal.pntd.0000729.
25. **Vannier-Santos MA, Menezes D, Oliveira MF, de Mello FG.** 2008. The putrescine analogue 1,4-diamino-2-butanone affects polyamine synthesis, transport, ultrastructure and intracellular survival in *Leishmania amazonensis*. Microbiology **154:**3104–3111. http://dx.doi.org/10.1099/mic.0.2007/013896-0.
26. **Rodrigues JC, Urbina JA, de Souza W.** 2005. Antiproliferative and ultrastructural effects of BPQ-OH, a specific inhibitor of squalene synthase, on *Leishmania amazonensis*. Exp. Parasitol. **111:**230–238. http://dx.doi.org/10.1016/j.exppara.2005.08.006.
27. **van Hellemond JA, Van Der Meer P, Tielens AGM.** 1997. *Leishmania infantum* promastigotes have a poor capacity for anaerobic functioning and depend mainly on respiration for their energy generation. Parasitology **114:**351–360. http://dx.doi.org/10.1017/S0031182096008591.
28. **de Souza W, Rodrigues JC.** 2009. Sterol biosynthesis pathway as target for anti-trypanosomatid drugs. Interdiscip. Perspect. Infect. Dis. **2009:**642502. http://dx.doi.org/10.1155/2009/642502.
29. **Fernandes Rodrigues JC, Concepcion JL, Rodrigues C, Caldera A, Urbina JA, de Souza W.** 2008. *In vitro* activities of ER-119884 and E5700, two potent squalene synthase inhibitors, against *Leishmania amazonensis*: antiproliferative, biochemical, and ultrastructural effects. Antimicrob. Agents Chemother. **52:**4098–4114. http://dx.doi.org/10.1128/AAC.01616-07.
30. **Coustou V, Besteiro S, Biran M, Diolez P, Bouchaud V, Voisin P, Michels PA, Canioni P, Baltz T, Bringaud F.** 2003. ATP generation in the *Trypanosoma brucei* procyclic form: cytosolic substrate level is essential but not oxidative phosphorylation. J. Biol. Chem. **278:**49625–49635. http://dx.doi.org/10.1074/jbc.M307872200.
31. **BoseDasgupta S, Das BB, Sengupta S, Ganguly A, Roy A, Dey S, Tripathi G, Dinda B, Majumder HK.** 2008. The caspase-independent algorithm of programmed cell death in *Leishmania* induced by baicalein: the role of LdEndoG, LdFEN-1 and LdTatD as a DNA 'degradesome'. Cell Death Differ. **15:**1629–1640. http://dx.doi.org/10.1038/cdd.2008.85.
32. **Schulze-Osthoff K, Bauer MK, Vogt M, Wesselborg S.** 1997. Oxidative stress and signal transduction. Int. J. Vitam. Nutr. Res. **67:**336–342.
33. **Carvalho L, Luque-Ortega JR, Manzano JI, Castanys S, Rivas L, Gamarro F.** 2010. Tafenoquine, an antiplasmodial 8-aminoquinoline, targets leishmania respiratory complex III and induces apoptosis. Antimicrob. Agents Chemother. **54:**5344–5351. http://dx.doi.org/10.1128/AAC.00790-10.
34. **Carvalho L, Luque-Ortega JR, López-Martín C, Castanys S, Rivas L, Gamarro F.** 2011. The 8-aminoquinoline analogue sitamaquine causes oxidative stress in *Leishmania donovani* promastigotes by targeting succinate dehydrogenase. Antimicrob. Agents Chemother. **55:**4204–4210. http://dx.doi.org/10.1128/AAC.00520-11.
35. **Mehta A, Shaha C.** 2004. Apoptotic death in *Leishmania donovani* promastigotes in response to respiratory chain inhibition: complex II inhibition results in increased pentamidine cytotoxicity. J. Biol. Chem. **279:**11798–11813. http://dx.doi.org/10.1074/jbc.M309341200.
36. **Sashidhara KV, Singh SP, Srivastava A, Puri A, Chhonker YS, Bhatta RS, Shah P, Siddiqi MI.** 2011. Discovery of a new class of HMG-CoA reductase inhibitor from *Polyalthia longifolia* as potential lipid lowering agent. Eur. J. Med. Chem. **46:**5206–5211. http://dx.doi.org/10.1016/j.ejmech.2011.08.012.
37. **Peña-Diaz J, Montalvetti A, Flores CL, Constán A, Hurtado-Guerrero R, De Souza W, Gancedo C, Ruiz-Perez LM, Gonzalez-Pacanowska D.** 2004. Mitochondrial localization of the mevalonate pathway enzyme

3-hydroxy-3-methyl-glutaryl-CoA reductase in the *Trypanosomatidae*. Mol. Biol. Cell **15:**1356–1363. http://dx.doi.org/10.1091/mbc.E03-10-0720.

38. **Montalvetti A, Peña-Díaz J, Hurtado R, Ruiz-Pérez LM, González-Pacanowska D.** 2000. Characterization and regulation of *Leishmania major* 3-hydroxy-3-methylglutaryl-CoA reductase. Biochem. J. **349:**27–34. http://dx.doi.org/10.1042/0264-6021:3490027.
39. **Kosec G, Alvarez VE, Agüero F, Sánchez D, Dolinar M, Turk B, Turk V, Cazzulo JJ.** 2006. Metacaspases of *Trypanosoma cruzi*: possible candidates for programmed cell death mediators. Mol. Biochem. Parasitol. **145:**18–28. http://dx.doi.org/10.1016/j.molbiopara.2005.09.001.
40. **Lee N, Gannavaram S, Selvapandiyan A, Debrabant A.** 2007. Characterization of metacaspases with trypsin-like activity and their putative role in programmed cell death in the protozoan parasite *Leishmania*. Eukaryot. Cell **6:**1745–1757. http://dx.doi.org/10.1128/EC.00123-07.
41. **Raina P, Kaur S.** 2012. Knockdown of LdMC1 and Hsp70 by antisense oligonucleotides causes cell-cycle defects and programmed cell death in *Leishmania donovani*. Mol. Cell. Biochem. **359:**135–149. http://dx.doi.org/10.1007/s11010-011-1007-y.
42. **Khademvatan S, Gharavi MJ, Saki J.** 2011. Miltefosine induces metacaspase and PARP genes expression in *Leishmania infantum*. Braz. J. Infect. Dis. **15:**442–448. http://dx.doi.org/10.1016/S1413-8670(11)70225-2.
43. **Phadnis AP, Patwardhan SA, Dhaneswar NN, Tavale SS, Row TNG.** 1988. Clerodane diterpenoids from *Polyalthia longifolia*. Phytochemistry **27:**2899–2901. http://dx.doi.org/10.1016/0031-9422(88)80684-8.
44. **Ichino C, Soonthornchareonnon N, Chuakul W, Kiyohara H, Ishiyama A, Sekiguchi H, Namatame M, Otoguro K, Omura S, Yamada H.** 2006. Screening of Thai medicinal plant extracts and their active constituents for *in vitro* antimalarial activity. Phytother. Res. **20:**307–309. http://dx.doi.org/10.1002/ptr.1850.
45. **Marthanda Murthy M, Subramanyam M, Hima Bindu M, Annapurna J.** 2005. Antimicrobial activity of clerodane diterpenoids from *Polyalthia longifolia* seeds. Fitoterapia **76:**336–339. http://dx.doi.org/10.1016/j.fitote.2005.02.005.
46. **Kerr JF, Wyllie AH, Currie AR.** 1972. Apoptosis: a basic biological phenomenon with wide-ranging implications in tissue kinetics. Br. J. Cancer **26:**239–257. http://dx.doi.org/10.1038/bjc.1972.33.